Inorganic Chemistry

pubs.acs.org/IC

Article

Photoinduced Generation of a Durable Thermal Proton Reduction Catalyst with in Situ Conversion of $Mn(bpy)(CO)_3Br$ to $Mn(bpy)_2Br_2$

Hunter Shirley, Sean Parkin, and Jared H. Delcamp*

Cite This: https://dx.doi.org/10.1021/acs.inorgchem.0c00480

Read Online

ACCESS | Metrics & More | Article Recommendations | Supporting Information

ABSTRACT: The conversion of protons to H_2 is a critical reaction for the design of renewable fuel generating systems. Robust, earth-abundant, metal-based catalysts that can rapidly facilitate this reduction reaction are highly desirable. $Mn(bpy)(CO)_3Br$ generates an active catalyst for the proton reduction reaction upon photolysis at a high, directly observed H_2 production rate of 1 300 000 turnovers per hour, with a low driving force for this reaction. Through the use of $FcMe_{10}$ as an electron source, a proton source (triflic acid, 4-cyanoanilinium, or tosylic acid), and $MeCN/H_2O$ as solvent, the thermal reaction at room temperature was found to proceed until complete consumption of the electron source. No apparent loss in catalytic activity was observed to the probed limit of 10 000 000 turnovers of H_2. Interestingly, a catalytically competent complex ($Mn(bpy)_2Br_2$), which could be isolated and characterized, formed upon photolysis of $Mn(bpy)(CO)_3Br$ in the presence of acid.

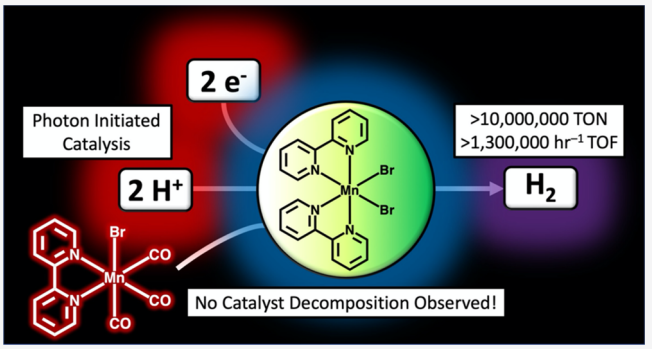

INTRODUCTION

The efficient storage of energy in chemical bonds for use on demand is a critical step forward in renewable fuel production.[1] Proton reduction to H_2 is a commonly pursued approach in the search for a chemical fuel that can be derived from an abundant resource such as water. If the hydrogen evolution reaction is paired with water oxidation, only O_2 is generated as a stoichiometric waste.[2] Ideally, these catalytic processes would be driven by robust catalysts derived from earth-abundant elements with fast rates of catalysis.[3,4] The catalysts should also durably operate with minimal driving force to avoid energetic losses.[3] Several reaction system designs coupling oxidative and reductive processes are reported in the literature surrounding electrochemical cells (EC) and photoelectrochemical cells (PEC), including those employing redox mediators, which can alleviate relative rate concerns of the anodic and cathodic reactions.[5−10] PEC and EC catalyst performances can be efficiently probed through the study of half reactions using a stoichiometric chemical electron source or sacrificial electron donor (SED). This approach is common in the literature and has led to the discovery of molecular catalysts used to drive reductive reaction processes in EC and PEC systems.[2,3,11−21] The use of an SED with reversible electron transfers (ETs) and no rapid chemical transformation step following the electron transfer step allows for the SED to potentially be used a redox mediator in full PEC/EC systems.[10]

Manganese bipyridyl complexes have recently been shown to catalyze proton reduction reactions[22] in addition to CO_2 reduction reactions.[23−25] Intriguingly, manganese tricarbonyl bromide complexes have been reported to dramatically change reactivity toward protons or CO_2 based on the addition of water,[23] and many of these complexes are reported under conditions that rigorously exclude light with red-light laboratory illumination being described in some literature instances as a needed precaution.[11,24,26−29] The use of dark conditions is interesting, since the literature suggests that discrete complexes are formed upon irradiation, which could be catalytically active in reduction reactions.[30] Whereas it can be difficult to isolate and confirm the identity of photogenerated compounds, the use of a photoinduced catalyst generation approach is convenient in that a simple to prepare starting complex can be transformed *in situ* to a new active catalyst for evaluation in the proton reduction reaction.

To probe the effects of light on $Mn(bpy)(CO)_3Br$ driven proton reduction reactions, a series of studies were performed using nuclear magnetic resonance (NMR), crystallography, infrared spectroscopy, electrochemical techniques, and thermal catalysis with an SED under varied conditions (Figure 1). For the thermal reduction reactions, a potential redox mediator, decamethylferrocene ($FcMe_{10}$), was selected as the sacrificial

Received: February 14, 2020

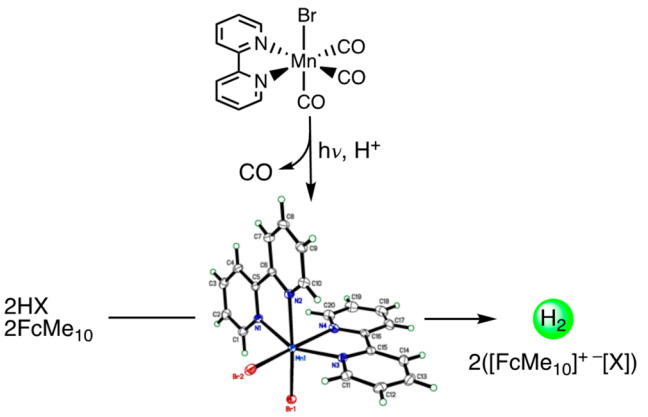

Figure 1. Photolytic CO dissociation from $Mn(bpy)(CO)_3Br$ (as shown by GC) to give $Mn(bpy)_2Br_2$ in the presence of protons. $Mn(bpy)_2Br_2$ is shown to facilitate the proton reduction reaction.

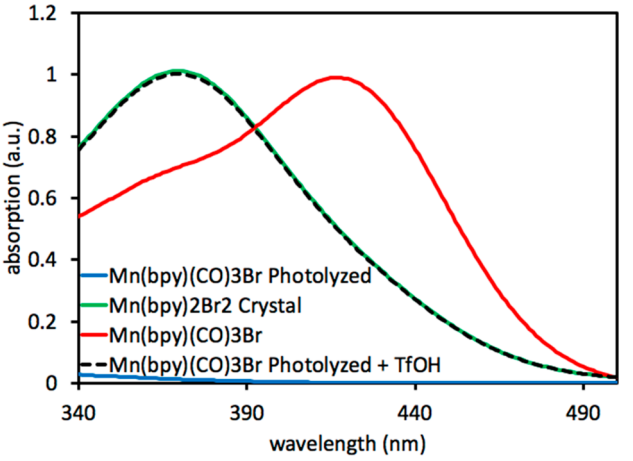

Figure 2. Absorption spectra of Mn complexes in MeCN before photolysis (red), after photolysis (blue), after photolysis with addition of TfOH (black), and after crystallization of $Mn(bpy)_2Br_2$ (green).

electron donor. This electron source was selected as a strongly reducing electron donor (−0.51 V versus Fc^+/Fc),[14] which leads to triflic acid in MeCN (2.6 pK_a)[31] resulting in an estimated exothermic reaction via the Nernst equation ($E = E^\circ - 0.059\ pK_a$) at a free energy of −0.33 V when the standard reduction potential of H^+ in MeCN is taken at −0.03 V versus Fc^+/Fc (eq 1, Figure S1).[32] The use of tosylic acid (8.6 pK_a in MeCN) results in an estimated slightly endothermic reaction at a free energy of +0.03 V (eq 3).[31,33,34] 4-Cyanoanilinium (7 pK_a in MeCN) was selected due to it being reasonably well-behaved under anhydrous conditions with a comparable intermediate free energy (−0.07 V) to the other acids in the reaction being probed (eq 2).[31,35] The reactions could be driven at room temperature, and the use of proton and electron sources without large driving forces for proton reduction allows for the indirect probing of the activation energy barrier of the catalyst in powering these reactions. Given the dramatic effects water has shown in Mn catalyzed CO_2 reduction reactions, water in varying amounts is also investigated.[23]

$$2TfOH + 2FcMe_{10} \rightarrow H_2 + 2[FcMe_{10}]^+[TfO]^- \quad \Delta G = -0.33V \quad (1)$$

$$2[NC\text{-}p\text{-}C_6H_4NH_3]^+[BF_4]^- + 2FcMe_{10} \rightarrow H_2 + 2NC\text{-}p\text{-}C_6H_4NH_2 + 2[FcMe_{10}]^+[BF_4]^- \quad \Delta G = -0.07\ V \quad (2)$$

$$2TsOH + 2FcMe_{10} \rightarrow H_2 + 2[FcMe_{10}]^+[TsO]^- \quad \Delta G = +0.03V \quad (3)$$

RESULTS AND DISCUSSION

As expected based on literature precedent,[30] the exposure of $Mn(bpy)(CO)_3Br$ to ambient light in MeCN leads to the quantitative loss of one CO ligand, as confirmed by GC in our laboratories. During this time, the solution of the complex changes from yellow to clear (Figures 2, S2 and S9, Table 1). This color change is diagnostic since $Mn(bpy)(CO)_3Br$ is known to dimerize to form $[Mn(bpy)(CO)_3]_2$ in non-coordinating solvents, and $[Mn(bpy)(CO)_3]_2$ has significant absorption spectrum features near 500, 650, and 850 nm.[36] These features are not present during ambient light photolysis in the presence of coordinating MeCN. Upon irradiation of $Mn(bpy)(CO)_3Br$ (red line), the absorption spectrum shows a quenching of the absorption at 422 nm and growth of the blue-shifted signal representative of the photolyzed, colorless solution (blue line in Figure 2; Figure S2). Upon the subsequent addition of TfOH, a signal at 370 nm arises, which is a new photogenerated complex (Figure 2). Additionally, ^1H NMR analysis of photolyzed $Mn(bpy)(CO)_3Br$ in CD_3CN shows NMR signals in a broad shape with a high signal-to-noise possibly due to the poor solubility of the photolyzed complex in MeCN or the generation of a paramagnetic complex with trace by-products generating the observed signals (Figures S3 and S4). Addition of TfOH to the NMR mixture after photolysis gives a by-product with sharp signals in the aromatic region not attributed to either the pre-photolyzed or post-photolyzed complex (Figure S5). No hydride signal was evident in the 0 to −70 ppm range. However, when TfOH, TsOH, or AcOH was added as an acid, the known complex $Mn(bpy)_2Br_2$,[37] could be obtained as X-ray quality crystals by evaporating the volatile components and taking the solids up in MeOH followed slow vapor diffusion of diethyl ether to give the crystalline complex at the top of the vial in high yield (>90% based on bpy, > 45% based on Mn). The structure was confirmed by crystallography at 90 K (Figure 1). Neither independently synthesized $Mn(bpy)_2Br_2$ nor that formed *in situ* gives paramagnetic ^1H NMR signals between 200 ppm and −200 ppm (Figure S6).

Absorption spectroscopy with $Mn(bpy)_2Br_2$ (green line) shows a matched absorption curve to the sample of $Mn(bpy)(CO)_3Br$ exposed to light and TfOH (black dashed line), indicating the complex is formed readily under the reaction conditions in solution (Figure 2). It is not apparent why the addition of an acid source is required to obtain the $Mn(bpy)_2Br_2$ complex. Additionally, attenuated total reflectance infrared spectroscopy (ATR-IR) confirms that the collected crystals no longer have a CO related signal in the 2100−1650 cm^{-1} region (Figures S10 and S11). Consistent with only one CO being observed extruding from the reaction mixture via gas chromatography (GC), the IR spectrum of the remaining material in the mother liquor shows numerous CO signals with broadened features in the 2100−1650 cm^{-1} region, which may be due to either a number of species being present or the formation of $Mn_x(CO)_y$-clusters (Figures

https://dx.doi.org/10.1021/acs.inorgchem.0c00480
Inorg. Chem. XXXX, XXX, XXX−XXX

Table 1. Electrochemical and Optical Data for $Mn(bpy)_2Br_2$ and $Mn(bpy)(CO)_3Br$[a]

complex	λ_{max} (nm)	λ_{onset} (nm)	$E_{red1\ no\ H+}$ (V) peak | onset	$E_{red2\ no\ H+}$ (V) peak | onset	$E_{red\ H+}$ (V) onset	i_{cat}/i_p
$Mn(bpy)(CO)_3Br$	422	485	— | −2.20	— | —	−1.25	13
photolyzed $Mn(bpy)(CO)_3Br$	302	325	−1.79 | −1.65	−1.97 | −1.85	−0.51	17
$Mn(bpy)_2Br_2$	371	375	−1.20 | −0.90	— | —	−0.55	23 (dark) 29 (light)

[a]All values are measured in MeCN. i_{cat}/i_p is calculated from the CV curve where i_{cat} is the peak current with TfOH present and i_p is the peak current without TfOH, with $Mn(bpy)(CO)_3Br$ measured at −1.75 V, the photoinduced catalyst measured at −0.80 V, and $Mn(bpy)_2Br_2$ measured at −1.20 V.

S10 and S11). This material is observed to absorb in the UV region (<350 nm), suggesting loss of any possible metal−ligand charge transfer bands due to loss of bipyridine (Figure S2). The IR spectrum further confirms near complete loss of bipyridine related features in the 1600−1400 cm^{-1} region. The fate of the remaining Mn atom after two $Mn(bpy)(CO)_3Br$ complexes are converted to $Mn(bpy)_2Br_2$ is not apparent. We note that two CO molecules are observed in the headspace via GC from two $Mn(bpy)(CO)_3Br$ complexes. This leaves four CO groups and a Mn atom needed to balance the stoichiometry of the transformation shown in Figure S12.

Subjecting the crystallized $Mn(bpy)_2Br_2$ to the chemical reaction conditions found to be catalytically competent gave H_2 at a very similar rate to photolyzed $Mn(bpy)(CO)_3Br$, although it should be noted that the rate of this system is likely SED solubility limited (see discussion below). Additionally, $Mn(bpy)(CO)_3Br$ and $Mn(bpy)_2Br_2$ prepared via independent methods gave the same aromatic NMR signals when the complex was exposed to TfOH and the reducing reagent $FcMe_{10}$ (Figures S7 and S8). Although it cannot be confirmed that the signals observed are not a by-product unrelated to catalysis, it is plausible that the paramagnetic $Mn(bpy)_2Br_2$ formed in the reaction mixture can be reduced to a diamagnetic Mn(I) compound. Notably, all components necessary for catalytic H_2 production are present once the reducing reagent and TfOH are added, which suggests the observed ^1H NMR signals may either be a by-product or the resting state of the catalyst. Importantly, both complexes appear to be doing the same chemistry given the same ^1H NMR spectrum is arrived at after proton and reducing reagent are added.

Electrochemically, a significant change in the reduction potential of $Mn(bpy)(CO)_3Br$ is observed after light exposure in MeCN (Figure 3 top: green line (dark), blue line (light), Table 1). A shift of 0.55 V toward a more positive potential is observed with a first reduction potential peak of −1.79 V for photolyzed $Mn(bpy)(CO)_3Br$ under argon (top: blue line). Even under conditions that rigorously exclude light, small amounts of the photolyzed product are present in the "dark" with $Mn(bpy)(CO)_3Br$. $Mn(bpy)_2Br_2$ shows a reduction wave onset near −0.9 V with a reduction wave peak at −1.20 V (top: black line). Introduction of a proton source (TfOH) leads to a shift toward more positive potentials for the $Mn(bpy)(CO)_3Br$ complex in the dark with an onset of −1.25 V, and a peak potential observed at −2.24 V after an initial plateau near −1.75 V (middle: green line (without TfOH), red line (with TfOH)). The observed shift in electrochemical potential in the dark suggests an initial chemical reaction has taken place resulting in a new species with a more positive reduction potential. The observed onset of reduction is estimated to be an overpotential of 1.07 V as calculated from standard reduction potential of protons in MeCN solvent at −0.18 V versus Fc^+/Fc with the pK_a of TfOH in MeCN taken at 2.6 and estimated through the Nernst equation (see above). The observed current enhancement is measured as an i_{cat}/i_p value of 13 at the first reduction's plateau (−1.75 V).[28,38] The photogenerated species shows a reduction potential onset near −0.51 V versus Fc^+/Fc in the presence of TfOH (middle: black line). This corresponds to an overpotential of only 0.32 V and occurs 0.75 V more positive than that observed with $Mn(bpy)(CO)_3Br$ under otherwise identical conditions (middle: red line). Additionally, a large shift in reduction potential onset (1.14 V) is observed when the CVs of photolyzed $Mn(bpy)(CO)_3Br$ with (middle: black line) and without (middle: blue line) TfOH are compared, which is consistent with the formation of a relatively electron deficient catalytically active complex upon the addition of TfOH. The observed current enhancement is representative of a 17× increase in current at the first reduction's plateau (−0.80 V) (Figure 3, see Figures S13−S16 for additional CV data).

Upon exposure of $Mn(bpy)_2(Br)_2$ to TfOH in the dark (bottom: red line) or in the light (bottom: black line), a current increase is observed (i_{cat}/i_p of 23 and 29, respectively) with a slight shoulder near the curve peak emerging, which is not apparent from the curve with $Mn(bpy)_2(Br)_2$ in the absence of TfOH (bottom: blue line) (Figure 3). No dramatic difference is observed in the light or dark when TfOH is present with respect to curve shape or current increase. The slight shoulder observed near −1.1 V and the reduction wave peak at −1.20 V with $Mn(bpy)_2(Br)_2$ match closely in potential to the two shoulder features observed when $Mn(bpy)(CO)_3Br$ is exposed to light and TfOH (bottom: green line). The features of the $Mn(bpy)(CO)_3Br$ voltammogram taken in the presence of light and TfOH (green line) appear to be comprised of the catalytic reduction wave features of the bipyridine free Mn material (gray line with TfOH, purple line without TfOH) and $Mn(bpy)_2Br_2$.

To confirm the current enhancement observed via CV is due to proton reduction, controlled potential electrolysis (CPE) studies were carried out at the initial current plateau potential observed via CV for photolyzed $Mn(bpy)(CO)_3Br$ in the presence of TfOH with a glassy carbon working electrode, glassy carbon counter electrode, and a silver wire reference electrode. Molecular hydrogen is produced with a Faradaic efficiency (FE) of 100% when applying a constant potential at the first reduction (−0.80 V) of photolyzed $Mn(bpy)(CO)_3Br$ (Figure 4, red line). However, at the same potential negligible molecular hydrogen relative to the background reaction (blue line) is produced when $Mn(bpy)(CO)_3Br$ is kept in the dark (black line). A steady rate of charge passing is observed over a 2 h time period for photolyzed $Mn(bpy)(CO)_3Br$ with no evidence of catalyst decomposition based on the lack of charge passage rate changes.

https://dx.doi.org/10.1021/acs.inorgchem.0c00480
Inorg. Chem. XXXX, XXX, XXX−XXX

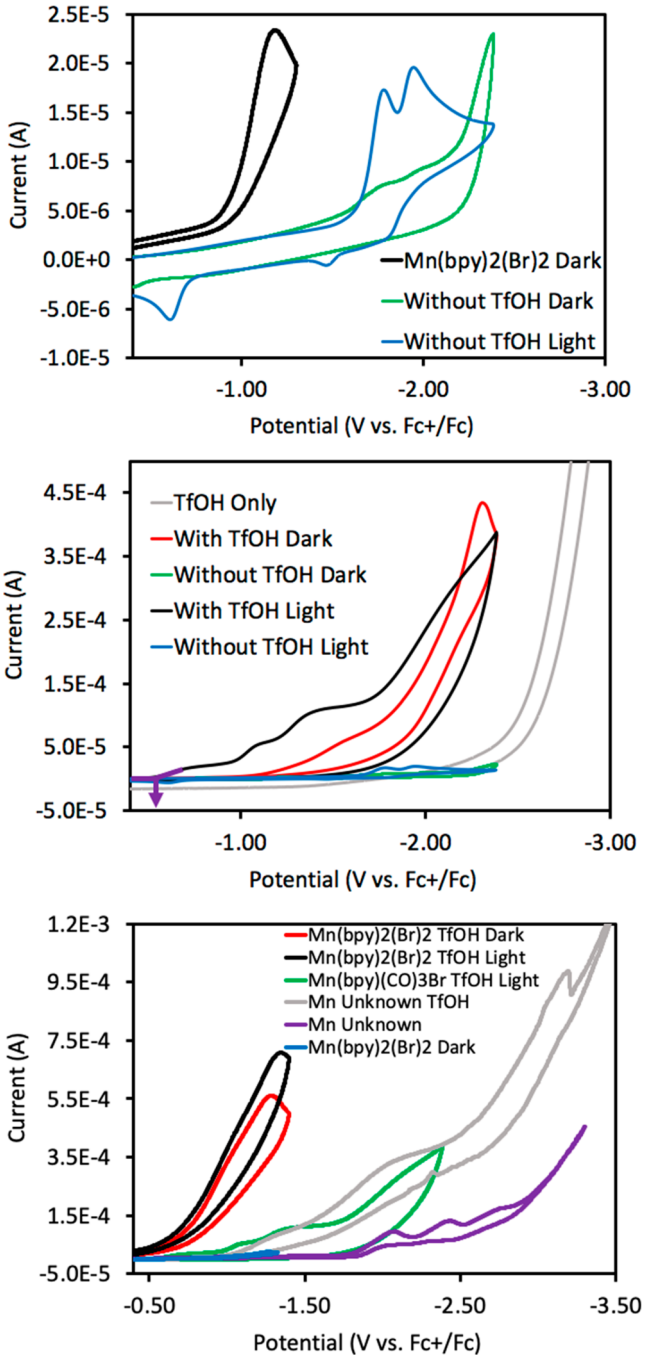

Figure 3. Top: CVs of $Mn(bpy)(CO)_3Br$ in the light or dark and $Mn(bpy)_2Br_2$, all without TfOH. Middle: Cyclic voltammograms for $Mn(bpy)(CO)_3Br$ at 1 mM (μmol cat/mL MeCN) in the light or dark and with or without 0.19 M TfOH present. Bottom: CVs with $Mn(bpy)_2Br_2$, $Mn(bpy)(CO)_2Br$, or the remaining Mn material after crystallization under varied conditions. A scan rate of 100 mV/s is used in all cases. The electrolyte is 0.1 M Bu_4NPF_6 in MeCN with glassy carbon working, platinum counter, and Ag-wire reference. The onset potentials in Table 1 are determined as shown by the purple arrow example on the middle graph.

Thermal catalytic studies with an SED ($FcMe_{10}$) were undertaken having found the resulting complex from irradiation of $Mn(bpy)(CO)_3Br$ to have desirable rates of proton reduction and favorable reaction energetics via electrochemical analysis. The use of a potential redox mediator as an SED is attractive in allowing for the probing of catalyst

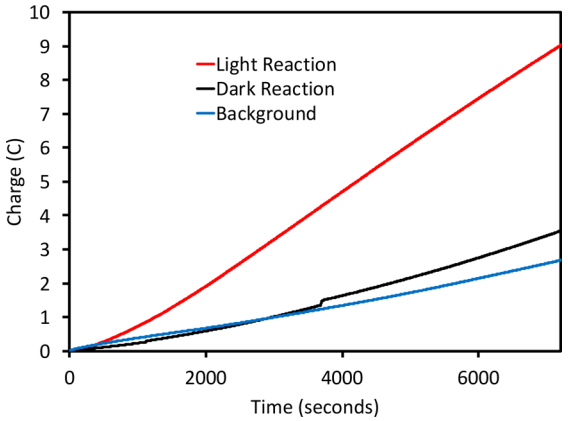

Figure 4. Charge passage over time graph for CPE experiments with $Mn(bpy)(CO)_3Br$ (black, 1 mM) and photolyzed $Mn(bpy)(CO)_3Br$ (red, 1 mM). The blue line is a background reaction with all components kept constant minus catalyst.

durability with an SED that could be rendered catalytic in EC/PEC systems.[5−10] $Mn(bpy)(CO)_3Br$ was first dissolved in MeCN and TfOH, then $FcMe_{10}$ was added in the dark. After 4 h, no appreciable H_2 was detected in the headspace (Figure 5,

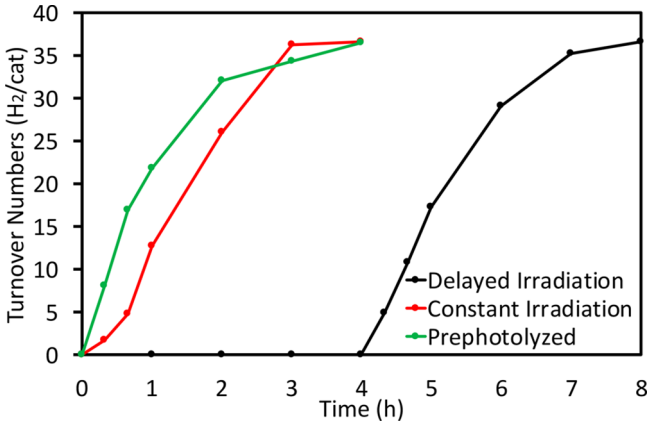

Figure 5. TON vs time under identical reaction conditions (0.1 mM catalyst, 0.19 M TfOH, 33.7 μmol of $FcMe_{10}$, and 2% H_2O), but with varying light exposure parameters. The black curve shows a reaction that was kept shielded from light for 4 h prior to being placed in front a solar simulator at 1 sun intensity. The red curve shows a reaction that was irradiated constantly. The green curve shows a reaction that was prephotolyzed before TfOH addition and then placed in the dark.

black line). Upon exposure to 1 sun intensity solar simulated light for 5 min, catalysis immediately began, with no additional irradiation needed and catalysis proceeded until a high yield (85%) of H_2 was observed with respect to the amount of $FcMe_{10}$ added assuming 2 $FcMe_{10}$ SED molecules are required per H_2 molecule produced (Table 2, entry 1). This corresponds to 29 turnover numbers (TONs) calculated via the equation TON = (H_2 mol/Mn-catalyst moles). A turnover frequency (TOF) of 81 h^{-1} is observed over the initial 20 min period of the reaction, according to the equation TOF = TON/time. The reaction was found to follow a near identical profile with respect to a TON versus time plot during continuous irradiation (red line) or irradiation prior to acid and SED addition (green line) indicating the reaction is photoinitiated without any significant deactivation pathway, which would require photons to access the active catalyst again

https://dx.doi.org/10.1021/acs.inorgchem.0c00480
Inorg. Chem. XXXX, XXX, XXX−XXX

Table 2. Reactions Performed with Photolyzed $Mn(bpy)(CO)_3Br$ or $Mn(bpy)_2Br_2$, $FcMe_{10}$ (33.7 μmol), and 0.19 M TfOH (or Replacement Acid) in MeCN (5 mL) for 4 h unless Otherwise Noted[a]

entry	[catalyst]	change	TON of H_2	TOF[b] (h^{-1})	H_2 yield[c]
		Benchmark Experiment and Controls			
1	0.1 mM	none	29	81	85%
2	none	no catalyst	<1	<1	0%
3	none	no catalyst, + 2% H_2O	<1	<1	0%
4	0.1 mM	no $FcMe_{10}$	<1	<1	0%
5	0.1 mM	no TfOH	<1	<1	0%
6	0.1 mM	−$FcMe_{10}$, + BIH[d]	<1	<1	0%
7	0.1 mM	−$FcMe_{10}$, + ferrocene	<1	<1	0%
		Acid Effects			
8[e]	0.1 mM	−TfOH, + $[NC\text{-}p\text{-}C_6H_4NH_3]^+$	25	8	74%
9	0.1 mM	−TfOH, + TsOH	22	12	65%
10	$Mn(bpy)_2Br_2$ (0.1 mM)	−TfOH, + TsOH	20	13	59%
11	0.1 mM	−TfOH, + TFA	<1	<1	0%
12	0.1 mM	−TfOH, + AcOH	<1	<1	0%
		H_2O Effects			
13	0.1 mM	+2% H_2O	34	24	quant.
14	0.1 mM	+5% H_2O	10	13	29%
15	0.1 mM	+10% H_2O	5	11	15%
		Catalyst Durability Evaluation			
16	0.01 mM	+2% H_2O	340	140	quant.
17	1.0 μM	+2% H_2O	3400	1,600	quant.
18	0.1 μM	+2% H_2O	34,000	16,000	quant.
19	0.01 μM	+2% H_2O	340,000	120,000	quant.
20	1.0 nM	+2% H_2O	3,400,000	1,100,000	quant.
21[f]	1.0 nM	+2% H_2O, 3× $FcMe_{10}$	10,000,000	1,300,000	quant.
22[f]	$Mn(bpy)_2Br_2$ 1.0 nM	+2% H_2O, 3× $FcMe_{10}$	10,000,000	1,300,000	quant.

[a]TON vs. time plots are shown in Figures S17−22. [b]TOF is calculated as an initial rate by taking a sample after the first 20 min of the reaction and dividing the observed TON by the time elapsed. Note: the TOF value only establishes a lower limit for catalytic rate (see discussion below), and the TON value for $Mn(bpy)(CO)_3Br$ is calculated with respect to the amount of starting complex rather than the amount of active catalyst formed. [c]% yield of H_2 is calculated based on the number of H_2 molecules observed divided by half the number of FcMe10 molecules present and multiplied by 100%. [d]1,3-Dimethyl-2-phenyl-2,3-dihydro-1H-benzo[d]imidazole (BIH) as a sacrificial reductant. [e]Reaction was monitored over 12 h. [f]Reaction was monitored over 22 h.

(i.e., continuous illumination is not necessary, Figure 5). Removal of the Mn catalyst, $FeMe_{10}$, or TfOH from the reaction mixture led to no appreciable H_2 formation (Table 2, entries 2−5; Figure S22). Exchange of the SED for either BIH or ferrocene led to no H_2 product formation, presumably due to these SEDs being less reducing, resulting in endothermic reactions with free energies of +0.08 V and +0.18 V, respectively (Table 2, entries 6−7; Figure S22).[12]

Exchange of the TfOH proton source for acids with higher pK_as was evaluated with 4-cyanoanilinium tetrafluoroborate, TsOH, trifluoroacetic acid (TFA), and acetic acid (AcOH) to examine the effects of changing the free energy of the reaction being catalyzed (Table 2, entries 8−12; Figure S20). The free energies for the proton reduction reactions with $FcMe_{10}$ are estimated at −0.07 V, + 0.03 V, + 0.78 V, and +1.42 V for 4-cyanoanilinium tetrafluoroborate, TsOH, TFA, and AcOH, respectively. Notably, the rate of chemical reduction with 4-cyanoanilinium is slowed relative that of TfOH (TOF of 8 versus 81 h^{-1}, respectively); however, the overall TON value is similar at 25 versus 29 for the reportedly more well-behaved 4-cyanoanilinium (Table 2, entry 8).[31] Interestingly, TsOH was found to be a competent proton source for this reaction, indicating the thermal energy present at room temperature is sufficient to overcome any activation energy barriers and drive this slightly endothermic reaction. A TON of 22 was observed for a 65% H_2 yield with respect to the SED. A slower TOF is observed with TsOH and photolyzed $Mn(bpy)(CO)_3Br$ to TfOH (12 versus 81 h^{-1}). Similarly, crystallographically characterized $Mn(bpy)_2Br_2$ was found to react TsOH for 20 TONs and a TOF of up to 13 h^{-1} (Table 2, entry 10; Figure S21). As expected, the larger endothermic reactions with TFA and AcOH gave no appreciable reactivity.

Water was explored as an additive for this reaction since $Mn(bpy)_3(CO)_3Br$ is known to undergo dramatic catalysis changes in the presence of H_2O.[23] Addition of 2% H_2O v/v with MeCN led to an increase in observed H_2 with a TON of 34 for a quantitative H_2 yield (Table 2, entry 13; Figure S19). The TOF of the reaction slowed by ∼4× upon water addition for this reaction, although it is not clear if this is due to a change in pK_a of the proton source with the new solvent medium changing the reaction energetics or some other role. Further increasing the percent composition of H_2O to 5% and 10% led to diminished TON values of 10 and 5 along with decreased percent yield values of H_2 at 29% to 15% and a dramatic slowing of catalyst TOF by 10× (Table 2, entries 14 and 15, Figure S19). This loss in reactivity may be due to changes in reaction energetics or additional loss of solubility of $FcMe_{10}$, which is already sparingly soluble in pure MeCN and reacts into solution in dry MeCN over time. The solubility of $FcMe_{10}$ is likely rate limiting under these conditions.

With optimal conditions identified for the proton reduction reaction, the catalyst durability was probed by decreasing the

https://dx.doi.org/10.1021/acs.inorgchem.0c00480
Inorg. Chem. XXXX, XXX, XXX−XXX

catalyst concentration and holding the remaining component concentrations constant (Table 2, entries 16–20; Figure S17). Interestingly, from 0.1 mM to 1.0 nM photolyzed $Mn(bpy)(CO)_3Br$ was found to quantitatively consume electrons from $FcMe_{10}$ to produce H_2 with up to 3 400 000 TONs observed with a TOF observed of >1 000 000 h^{-1}. Given that complete consumption of $FcMe_{10}$ is turnover limiting, CPE was attempted with $FcMe_{10}$ to probe if an increase in H_2 generation rate electrochemically could be observed with an added redox shuttle that might have advantageous interfacial electron transfer kinetics at an electrode surface relative to the active catalyst; however, catalysis was found to slow during electrolysis when $FcMe_{10}$ was added due to electrode fouling as a result of the limited solubility of $FcMe_{10}$. The near linear changes in TOF across the 5 orders of magnitude in catalyst concentrations probed in the thermal reaction suggests that the reaction rate is likely limited by the relative concentration of the electron source in solution under optimized conditions. The solubility limit of $FcMe_{10}$ is estimated at 1 mg per 75 mL of MeCN, and solid $FeMe_{10}$ can be observed reacting into solution over time. To assess the catalyst durability limits, a large excess of $FcMe_{10}$ was added, and a TON value of ~10 000 000 was observed with a TOF value of 1 300 000 h^{-1} (Table 2, entry 21; Figure S18). The same values are observed with $Mn(bpy)_2Br_2$ as the starting complex (Table 2, entry 22). The leveling off of TOF after dramatically increasing the amount of $FcMe_{10}$ while holding catalyst concentration constant further suggests the electron source solubility is limiting catalytic rates. Thus, the reported TOF values can only be used to establish a lower limit catalyst TOF under the optimized conditions since the maximum rate cannot be observed due to the limited solubility of $FeMe_{10}$. Notably, the TOF and TON values in Table 2 can be effectively doubled when starting with $Mn(bpy)(CO)_3Br$ since $Mn(bpy)_2Br_2$ is formed seeming cleanly under the reaction conditions in >90% yield relative to bpy ligand and displays very similar reactivity.

CONCLUSION

$Mn(bpy)(CO)_3Br$ was shown to photolyze to a new catalyst for H^+ reduction. Upon addition of H^+, $Mn(bpy)_2(Br)_2$ could be crystallized after photolysis of $Mn(bpy)(CO)_3Br$, and upon subjecting these crystals to the reaction conditions, similar reactivity was observed for $Mn(bpy)(CO)_3Br$ in the same reaction conditions. The photogenerated catalyst was found to catalyze the reduction of protons at a lower potential and a larger i_{cat}/i_p ratio than $Mn(bpy)(CO)_3Br$ via cyclic voltammetry and controlled potential electrolysis. In a thermal reaction setup, the photoinduced species was found to be exceptionally durable with >10 000 000 TON observed and a fast catalysis TOF of 1 300 000 h^{-1} directly observed from the H_2 amount formed. Decomposition of the catalyst was not observed in these studies. This is a relatively rapid, durable catalytic system, which powers the low overpotential, thermal reaction of TsOH with $FeMe_{10}$ at about +0.03 eV. Future work is aimed at characterizing the intermediates involved in the process and integration of this catalyst into a full PEC/EC system for water splitting.

ASSOCIATED CONTENT

Supporting Information

The Supporting Information is available free of charge at https://pubs.acs.org/doi/10.1021/acs.inorgchem.0c00480.

Experimental details, additional spectroscopic information, catalysis experiments (PDF)

Accession Codes

CCDC 2003559 contains the supplementary crystallographic data for this paper. These data can be obtained free of charge via www.ccdc.cam.ac.uk/data_request/cif, or by emailing data_request@ccdc.cam.ac.uk, or by contacting The Cambridge Crystallographic Data Centre, 12 Union Road, Cambridge CB2 1EZ, UK; fax: +44 1223 336033.

AUTHOR INFORMATION

Corresponding Author

Jared H. Delcamp − *Department of Chemistry and Biochemistry, University of Mississippi, University, Mississippi 38677, United States;* orcid.org/0000-0001-5313-4078; Email: delcamp@olemiss.edu

Authors

Hunter Shirley − *Department of Chemistry and Biochemistry, University of Mississippi, University, Mississippi 38677, United States;* orcid.org/0000-0002-6224-556X

Sean Parkin − *Department of Chemistry, University of Kentucky, Lexington, Kentucky 40506, United States;* orcid.org/0000-0001-5777-3918

Complete contact information is available at: https://pubs.acs.org/10.1021/acs.inorgchem.0c00480

Funding

This work is supported by NSF Award 1800281. The D8 Venture diffractometer at the University of Kentucky was funded by the NSF (MRI CHE-1625732).

Notes

The authors declare no competing financial interest.

REFERENCES

(1) Benson, E. E.; Kubiak, C. P.; Sathrum, A. J.; Smieja, J. M. Electrocatalytic and Homogeneous Approaches to Conversion of CO_2 to Liquid Fuels. *Chem. Soc. Rev.* **2009**, *38*, 89–99.

(2) Hammer, N. I.; Sutton, S.; Delcamp, J. H.; Graham, J. D. Photocatalytic Water Splitting and Carbon Dioxide Reduction. In *Handbook of Climate Change Mitigation and Adaptation*; Chen, W. Y., Suzuki, T., Lackner, M., Eds.; Springer, 2017; DOI: 10.1007/978-3-319-14409-2_46.

(3) Fukuzumi, S.; Lee, Y.-M.; Nam, W. Thermal and Photocatalytic Production of Hydrogen with Earth-Abundant Metal Complexes. *Coord. Chem. Rev.* **2018**, *355*, 54–73.

(4) Dalle, K. E.; Warnan, J.; Leung, J. J.; Reuillard, B.; Karmel, I. S.; Reisner, E. Electro- and Solar-Driven Fuel Synthesis with First Row Transition Metal Complexes. *Chem. Rev.* **2019**, *119*, 2752–2875.

(5) Walter, M. G.; Warren, E. L.; McKone, J. R.; Boettcher, S. W.; Mi, Q.; Santori, E. A.; Lewis, N. S. Solar Water Splitting Cells. *Chem. Rev.* **2010**, *110*, 6446–6473.

(6) Kim, J. H.; Hansora, D.; Sharma, P.; Jang, J. W.; Lee, J. S. Toward Practical Solar Hydrogen Production - an Artificial Photosynthetic Leaf-to-Farm Challenge. *Chem. Soc. Rev.* **2019**, *48*, 1908–1971.

(7) Sankir, N. D.; Sankir, M. *Photoelectrochemical Solar Cells*; Scrivener Publishing LLC, 2018; Section 1.6.1.3, DOI: 10.1002/9781119460008.

(8) Kong, D.; Zheng, Y.; Kobielusz, M.; Wang, Y.; Bai, Z.; Macyk, W.; Wang, X.; Tang, J. Recent Advances in Visible Light-Driven Water Oxidation and Reduction in Suspension Systems. *Mater. Today* **2018**, *21*, 897–924.

(9) Maeda, K.; Domen, K. Photocatalytic Water Splitting: Recent Progress and Future Challenges. *J. Phys. Chem. Lett.* **2010**, *1*, 2655−2661.
(10) Sasaki, Y.; Kato, H.; Kudo, A. $[Co(bpy)_3]^{(3+/2+)}$ and $[Co(phen)_3]^{(3+/2+)}$ Electron Mediators for Overall Water Splitting under Sunlight Irradiation Using Z-Scheme Photocatalyst System. *J. Am. Chem. Soc.* **2013**, *135*, 5441−5449.
(11) Walsh, J. J.; Forster, M.; Smith, C. L.; Neri, G.; Potter, R. J.; Cowan, A. J. Directing the Mechanism of CO_2 Reduction by a Mn Catalyst through Surface Immobilization. *Phys. Chem. Chem. Phys.* **2018**, *20*, 6811−6816.
(12) Rodrigues, R. R.; Boudreaux, C. M.; Papish, E. T.; Delcamp, J. H. Photocatalytic Reduction of CO_2 to CO and Formate: Do Reaction Conditions or Ruthenium Catalysts Control Product Selectivity? *ACS Appl. Energy Mater.* **2019**, *2*, 37−46.
(13) Huckaba, A. J.; Sharpe, E. A.; Delcamp, J. H. Photocatalytic Reduction of CO_2 with Re-Pyridyl-NHCs. *Inorg. Chem.* **2016**, *55*, 682−690.
(14) Huckaba, A. J.; Shirley, H.; Lamb, R. W.; Guertin, S.; Autry, S.; Cheema, H.; Talukdar, K.; Jones, T.; Jurss, J. W.; Dass, A.; Hammer, N. I.; Schmehl, R. H.; Webster, C. E.; Delcamp, J. H. A Mononuclear Tungsten Photocatalyst for H_2 Production. *ACS Catal.* **2018**, *8*, 4838−4847.
(15) Du, P.; Schneider, J.; Luo, G.; Brennessel, W. W.; Eisenberg, R. Visible Light-Driven Hydrogen Production from Aqueous Protons Catalyzed by Molecular Cobaloxime Catalysts. *Inorg. Chem.* **2009**, *48*, 4952−4962.
(16) McCormick, T. M.; Han, Z.; Weinberg, D. J.; Brennessel, W. W.; Holland, P. L.; Eisenberg, R. Impact of Ligand Exchange in Hydrogen Production from Cobaloxime-Containing Photocatalytic Systems. *Inorg. Chem.* **2011**, *50*, 10660−10666.
(17) Wang, W.; Rauchfuss, T. B.; Bertini, L.; Zampella, G. Unsensitized Photochemical Hydrogen Production Catalyzed by Diiron Hydrides. *J. Am. Chem. Soc.* **2012**, *134*, 4525−4528.
(18) Esswein, A. J.; Nocera, D. G. Hydrogen Production by Molecular Photocatalysis. *Chem. Rev.* **2007**, *107*, 4022−4047.
(19) Windisch, J.; Orazietti, M.; Hamm, P.; Alberto, R.; Probst, B. General Scheme for Oxidative Quenching of a Copper Bis-Phenanthroline Photosensitizer for Light-Driven Hydrogen Production. *ChemSusChem* **2016**, *9*, 1719−1726.
(20) Khnayzer, R. S.; McCusker, C. E.; Olaiya, B. S.; Castellano, F. N. Robust Cuprous Phenanthroline Sensitizer for Solar Hydrogen Photocatalysis. *J. Am. Chem. Soc.* **2013**, *135*, 14068−14070.
(21) Utschig, L. M.; Silver, S. C.; Mulfort, K. L.; Tiede, D. M. Nature-Driven Photochemistry for Catalytic Solar Hydrogen Production: A Photosystem I-Transition Metal Catalyst Hybrid. *J. Am. Chem. Soc.* **2011**, *133*, 16334−16337.
(22) Sampson, M. D.; Kubiak, C. P. Electrocatalytic Dihydrogen Production by an Earth-Abundant Manganese Bipyridine Catalyst. *Inorg. Chem.* **2015**, *54*, 6674−6676.
(23) Bourrez, M.; Molton, F.; Chardon-Noblat, S.; Deronzier, A. $[Mn(bipyridyl)(CO)_3Br]$: An Abundant Metal Carbonyl Complex as Efficient Electrocatalyst for CO_2 Reduction. *Angew. Chem., Int. Ed.* **2011**, *50*, 9903−9906.
(24) Sampson, M. D.; Kubiak, C. P. Manganese Electrocatalysts with Bulky Bipyridine Ligands: Utilizing Lewis Acids to Promote Carbon Dioxide Reduction at Low Overpotentials. *J. Am. Chem. Soc.* **2016**, *138*, 1386−1393.
(25) Sinopoli, A.; La Porte, N. T.; Martinez, J. F.; Wasielewski, M. R.; Sohail, M. Manganese Carbonyl Complexes for CO_2 Reduction. *Coord. Chem. Rev.* **2018**, *365*, 60−74.
(26) Stanton, C. J., 3rd; Vandezande, J. E.; Majetich, G. F.; Schaefer, H. F., 3rd; Agarwal, J. Mn-NHC Electrocatalysts: Increasing π Acidity Lowers the Reduction Potential and Increases the Turnover Frequency for CO_2 Reduction. *Inorg. Chem.* **2016**, *55*, 9509−9512.
(27) Agarwal, J.; Shaw, T. W.; Stanton, C. J., 3rd; Majetich, G. F.; Bocarsly, A. B.; Schaefer, H. F., 3rd. NHC-Containing Manganese(I) Electrocatalysts for the Two-Electron Reduction of CO_2. *Angew. Chem., Int. Ed.* **2014**, *53*, 5152−5155.
(28) Agarwal, J.; Shaw, T. W.; Schaefer, H. F., III; Bocarsly, A. B. Design of a Catalytic Active Site for Electrochemical CO_2 Reduction with Mn(I)-Tricarbonyl Species. *Inorg. Chem.* **2015**, *54*, 5285−5294.
(29) Vollmer, M. V.; Machan, C. W.; Clark, M. L.; Antholine, W. E.; Agarwal, J.; Schaefer, H. F., 3rd; Kubiak, C. P.; Walensky, J. R. Synthesis, Spectroscopy, and Electrochemistry of (Alpha-Diimine)M-$(CO)_3$Br, M = Mn, Re, Complexes: Ligands Isoelectronic to Bipyridyl Show Differences in CO_2 Reduction. *Organometallics* **2015**, *34*, 3−12.
(30) Yempally, V.; Moncho, S.; Hasanayn, F.; Fan, W. Y.; Brothers, E. N.; Bengali, A. A. Ancillary Ligand Effects Upon the Photochemistry of $Mn(bpy)(CO)_3X$ Complexes (X = Br(−), PhCC(−)). *Inorg. Chem.* **2017**, *56*, 11244−11253.
(31) McCarthy, B. D.; Martin, D. J.; Rountree, E. S.; Ullman, A. C.; Dempsey, J. L. Electrochemical Reduction of Bronsted Acids by Glassy Carbon in Acetonitrile-Implications for Electrocatalytic Hydrogen Evolution. *Inorg. Chem.* **2014**, *53*, 8350−8361.
(32) Pegis, M. L.; Roberts, J. A.; Wasylenko, D. J.; Mader, E. A.; Appel, A. M.; Mayer, J. M. Standard Reduction Potentials for Oxygen and Carbon Dioxide Couples in Acetonitrile and N, N-Dimethylformamide. *Inorg. Chem.* **2015**, *54*, 11883−11888.
(33) Su, B.; Hatay, I.; Ge, P. Y.; Mendez, M.; Corminboeuf, C.; Samec, Z.; Ersoz, M.; Girault, H. H. Oxygen and Proton Reduction by Decamethylferrocene in Non-Aqueous Acidic Media. *Chem. Commun.* **2010**, *46*, 2918−2919.
(34) Su, B.; Hatay, I.; Li, F.; Partovi-Nia, R.; Méndez, M. A.; Samec, Z.; Ersoz, M.; Girault, H. H. Oxygen Reduction by Decamethylferrocene at Liquid/Liquid Interfaces Catalyzed by Dodecylaniline. *J. Electroanal. Chem.* **2010**, *639*, 102−108.
(35) Salnikov, G. E.; Genaev, A. M.; Vasiliev, V. G.; Shubin, V. G. Interaction of Acetonitrile with Trifluoromethanesulfonic Acid: Unexpected Formation of a Wide Variety of Structures. *Org. Biomol. Chem.* **2012**, *10*, 2282−2288.
(36) Stor, G. J.; Morrison, S. L.; Stufkens, D. J.; Oskam, A. The Remarkable Photochemistry of fac-$XMn(CO)_3$(.alpha.-diimine) (X = Halide): Formation of $Mn_2(CO)_6$(.alpha.-diimine)$_2$ Via the Mer Isomer and Photocatalytic Substitution of X- in the Presence of PR3. *Organometallics* **1994**, *13*, 2641−2650.
(37) Hwang, I.-C.; Ha, K. Crystal Structure of Bis(2,2′-Bipyridine-N,N′)Dibromomanganese(II), $MnBr_2(C_{10}H_8N_2)_2$. *Z. Kristallogr. NCS* **2007**, *222*, 209−210.
(38) Liyanage, N. P.; Dulaney, H. A.; Huckaba, A. J.; Jurss, J. W.; Delcamp, J. H. Electrocatalytic Reduction of CO_2 to CO with Re-Pyridyl-NHCs: Proton Source Influence on Rates and Product Selectivities. *Inorg. Chem.* **2016**, *55*, 6085−6094.

https://dx.doi.org/10.1021/acs.inorgchem.0c00480
Inorg. Chem. XXXX, XXX, XXX−XXX